

A new apparatus for modelling excavations

Sze Yue Lam

Research Associate, University of Cambridge, Cambridge, UK

Mohammed Z. E. B. Elshafie

Research Associate, University of Cambridge, Cambridge, UK

Stuart K. Haigh

Lecturer, University of Cambridge, Cambridge, UK

Malcolm D. Bolton

Professor, University of Cambridge, Cambridge, UK

Underground space is commonly exploited both to maximise the utility of costly land in urban development and to reduce the vertical load acting on the ground. Deep excavations are carried out to construct various types of underground infrastructure such as deep basements, subways and service tunnels. Although the soil response to excavation is known in principle, designers lack practical calculation methods for predicting both short- and long-term ground movements. As the understanding of how soil behaves around an excavation in both the short and long term is insufficient and usually empirical, the judgements used in design are also empirical and serious accidents are common. To gain a better understanding of the mechanisms involved in soil excavation, a new apparatus for the centrifuge model testing of deep excavations in soft clay has been developed. This apparatus simulates the field construction sequence of a multi-propped retaining wall during centrifuge flight. A comparison is given between the new technique and the previously used method of draining heavy fluid to simulate excavation in a centrifuge model. The new system has the benefit of giving the correct initial ground conditions before excavation and the proper earth pressure distribution on the retaining structures during excavation, whereas heavy fluid only gives an earth pressure coefficient of unity and is unable to capture any changes in the earth pressure coefficient of soil inside the zone of excavation, for example owing to wall movements. Settlements of the ground surface, changes in pore water pressure, variations in earth pressure, prop forces and bending moments in the retaining wall are all monitored during excavation. Furthermore, digital images taken of a cross-section during the test are analysed using particle image velocimetry to illustrate ground deformation and soil–structure interaction mechanisms. The significance of these observations is discussed.

Notation

D_{10}	diameter of the soil particles for which 10% of the particles are finer
D_{50}	mean grain size
D_{60}	diameter of the soil particles for which 60% of the particles are finer
EI	bending stiffness of the retaining wall
H	excavation depth
H_f	final excavation depth
K	coefficient of earth pressure
K_a	coefficient of earth pressure at active failure state
K_o	coefficient of earth pressure at rest
K_p	coefficient of earth pressure at passive failure state
s	prop spacing
s_u	undrained shear strength
γ_t	unit weight of soil
γ_w	unit weight of water
σ_h	horizontal total stress

σ_{ho} horizontal total stress at rest before excavation

σ_v vertical total stress

σ'_v vertical effective stress

1. Introduction

In order to obtain the reliable data that are essential for a better understanding of the behaviour of soils during the process of excavation, the simulation of that process should be realistic and reproducible. Although the instrumentation of actual excavations in the field is authoritative for the particular structure concerned, a major drawback to using field data in a scientific study is the difficulty of accurately characterising the soils that are present. Soil conditions and construction sequence will differ from site to site, and no experiment can hence ever be repeated. Furthermore, it would require an extraordinary array of inclinometers and extensometers to define the complete deformation mechanism of the ground.

However, field measurements remain important as a means of calibration and verification of any calculations that emerge from physical and numerical model studies.

The most widely attempted method of assessing soil–structure interaction problems is by continuum numerical analysis, using finite-element or finite-difference computer programs. These offer powerful tools to model complex construction processes, with a chosen structural system progressively put in place within a detailed ground stratigraphy. However, the ability to predict ground movements reliably is wholly dictated by the input of representative parameters for the various soils, and existing numerical codes are extremely demanding of such prior information. A more practical alternative is to discover simplified mechanisms of behaviour, and to use those in decision making. Such mechanisms universally form the basis of judgements that engineers make regarding possible collapse, but there has been relatively little information available on mechanisms that can be used to predict deformations under working conditions. The first step must be to observe them.

Small-scale centrifuge models can be used to simulate the prototype behaviour of an excavation in soil. A centrifugal acceleration field is used in a small-scale model to match the stresses induced by gravity in the prototype. The principal challenges are to design a test package to simulate the construction sequence of a braced excavation in the field, so that a cross-section can be used for the remote measurement of the resulting ground movements. The advantage is that tests can be repeated with planned variations, and that the model can be observed continuously from the occurrence of small deformations up to complete collapse, which is generally not allowed to happen in the field.

To model an excavation in a centrifuge, some method must be found of simulating soil removal in flight. The following four methods have been previously used to model in-flight excavation in a centrifuge

- (a) increasing centrifugal acceleration until failure (Lyndon and Schofield, 1970)
- (b) draining of a heavy fluid (Bolton and Powrie, 1987; Powrie, 1986)
- (c) removal of a bag of material from the excavation area (Azevedo, 1983)
- (d) an in-flight excavator (Kimura *et al.*, 1993; Loh *et al.*, 1998; Takemura *et al.*, 1999).

In the first method, soil in the excavation area is initially removed during model-making at $1g$, before the model is subjected to increasing centrifuge acceleration up to failure. Although the total vertical stress in a prototype can ultimately be reproduced, the scale factor continually changes with the

acceleration, and it is not possible to simulate the progressive ground movements owing to excavation in the field.

For the second method employed, the key idea is to replace the soil to be excavated by a fluid of identical density, retained in a rubber bag. The main drawback of simulation using a fluid is that the coefficient of lateral stress (K) is always one. This may approximate earth pressures adjacent to a cast-in-place wall (Richard *et al.*, 2006), but it would not be an appropriate technique for sheet pile walls inserted into clays, whether normally consolidated ($K_o < 1$) or heavily overconsolidated ($K_o > 1$). Even so it must be recognised that, during the excavation, K within the zone of future excavation will remain at unity in a heavy fluid, which is not consistent with what happens in the field where K below the excavation level may approach the passive earth pressure coefficient K_p . Thus, the technique of using liquid does not correctly reproduce the prototype deformations and stresses with respect to the progress of excavation.

In the third method, soil bags were placed in the zone to be excavated and were removed during the excavation process. This has one advantage over the first two methods, as the modelling of stress history is more realistic. Since the soil used in the bags is similar to the soil in the rest of the model, the initial coefficient of lateral stress should be consistent. Nonetheless, the interaction between the interfaces of the soil bags and the retaining wall would be very difficult to quantify.

Therefore, the first three methods cannot satisfactorily model a field excavation in clay soil in the centrifuge because the process of soil removal has not correctly been simulated. In view of this, in-flight excavation and bracing methods should be developed. Previous types of in-flight excavator modelled open cuttings with retaining walls, with or without ties that were placed initially at $1g$ (Loh *et al.*, 1998; Takamura *et al.*, 1999). These excavators produced interesting results, but the modelling of more realistic construction sequences that include wall and prop installation remains a challenge for physical modellers.

2. In-flight excavator

A new two-axis servo actuator was designed for the Turner beam centrifuge at Cambridge University (Haigh *et al.*, 2010). The actuator can apply a maximum load of 10 kN in vertical and horizontal directions, with a maximum speed of 5 mm/s, at an in-flight acceleration up to $100g$. The stroke of the equipment allows a maximum vertical displacement of 300 mm and a maximum horizontal displacement of 500 mm, monitored by encoders. The characteristics of the two-dimensional (2D) servo actuator are summarised in Table 1. Figure 1 shows the assembled excavator. The two

Maximum operating <i>g</i> -level	100 <i>g</i>
Actuator mass	150 kg
Horizontal displacement	500 mm
Maximum horizontal force	10 kN
Horizontal maximum velocity	5 mm/s
Vertical displacement	300 mm
Vertical maximum force	10 kN
Vertical maximum velocity	5 mm/s

Table 1. Capability of the two-axis actuator

DC servo-controlled motor-encoder units drive step-down gearboxes to increase the torque. Ball screws are used to convert these rotary motions into linear vertical and horizontal movements. The vertical screw system drives a ball nut carrier plate which slides along vertical guide rails, while the horizontal screw system shifts the whole actuator housing along horizontal guide rails. The whole frame was designed to be stiff enough to ensure good control of movements.

3. Experimental set-up

Figure 2 shows the experimental set-up of the present study. The rectangular model container is made of aluminium alloy with internal dimensions 790 mm long, 180 mm wide and 470 mm deep. The front face of the container consists of a poly(methyl methacrylate) (PMMA) window, which enables the whole testing process to be monitored by cameras mounted in front. The back of the container has holes at specific locations with respect to the position of the retaining wall, for the installation of pore pressure transducers and the provision of drainage. The servo actuator stands above the rim of the model container. The carrier plate of the actuator is connected through a screw fitting to an inverted T-shaped scraper which performs in-flight excavation at 60*g*.

Instrumentation comprising pore pressure transducers in the soil, earth pressure cells on the retaining wall, bending moment strain gauges on the wall, load cells on the props, laser sensors and linear variable transformers for displacement measurements were installed. Digital cameras were mounted in front of the PMMA window and LED (light-emitting diode) arrays were situated to illuminate the clay cross-section without causing glare or shadows.

In this paper, the results of two centrifuge tests on excavations with different support system stiffness are discussed. For test 1, a 6 mm thick aluminium plate is used to model an excavation with a 1.1 m thick diaphragm wall. For test 2, a 2 mm thick plate is used to model excavation using a sheet pile wall. The test programme is summarised in Table 2.

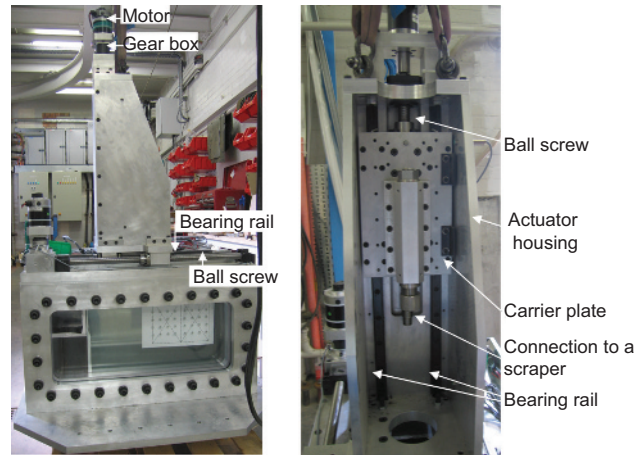


Figure 1. In-flight excavator

4. Cylinder support system and gate system

The vertical plane through the centre of an excavation can be regarded as a plane of symmetry. A ‘gate wall’ (as shown in Figure 3) aims to represent this plane of symmetry, so that only one side of the excavation needs to be modelled. Polytetrafluoroethylene (PTFE) sheets are glued on the gate wall to minimise vertical friction, and steps are also taken to prevent its lateral movement prior to excavation.

A prop installation subsystem was designed to provide in-flight support, initially to the gate wall and ultimately to the retaining wall, during the experiment. Three pairs of cylinders (Festo DSNU 25–125) are mounted on a rigid support frame and positioned at 0 mm, 36 mm and 72 mm below the initial clay surface. Props are driven by way of pistons in the cylinders which are actuated through a hydraulic/pneumatic control system. Backward pressure inlets are connected to a compressed air source for retreating the cylinders. Forward pressure inlets are connected to an oil pressure reservoir so that they can provide a similar propping force at each excavation level. Each level of props is controlled individually through solenoid valves. The oil supply manifold is connected to an air–oil interface through a needle valve, which is used to control the rate of advance of each pair of props, in sequence. Compressed air acting on the front face of the pistons is transmitted from an external compressor and regulator, and is supplied to the centrifuge through a pneumatic coupling.

Before the experiment, the system is saturated with hydraulic oil. The prop stiffness is obtained by conducting axial-load displacement tests in a loading rig. The target stiffness of a fully saturated prop is found to be about 1.66 kN/mm. To begin with, all pressure sources are at atmospheric pressure. All solenoid valves are closed. The advancing of a pair of props is

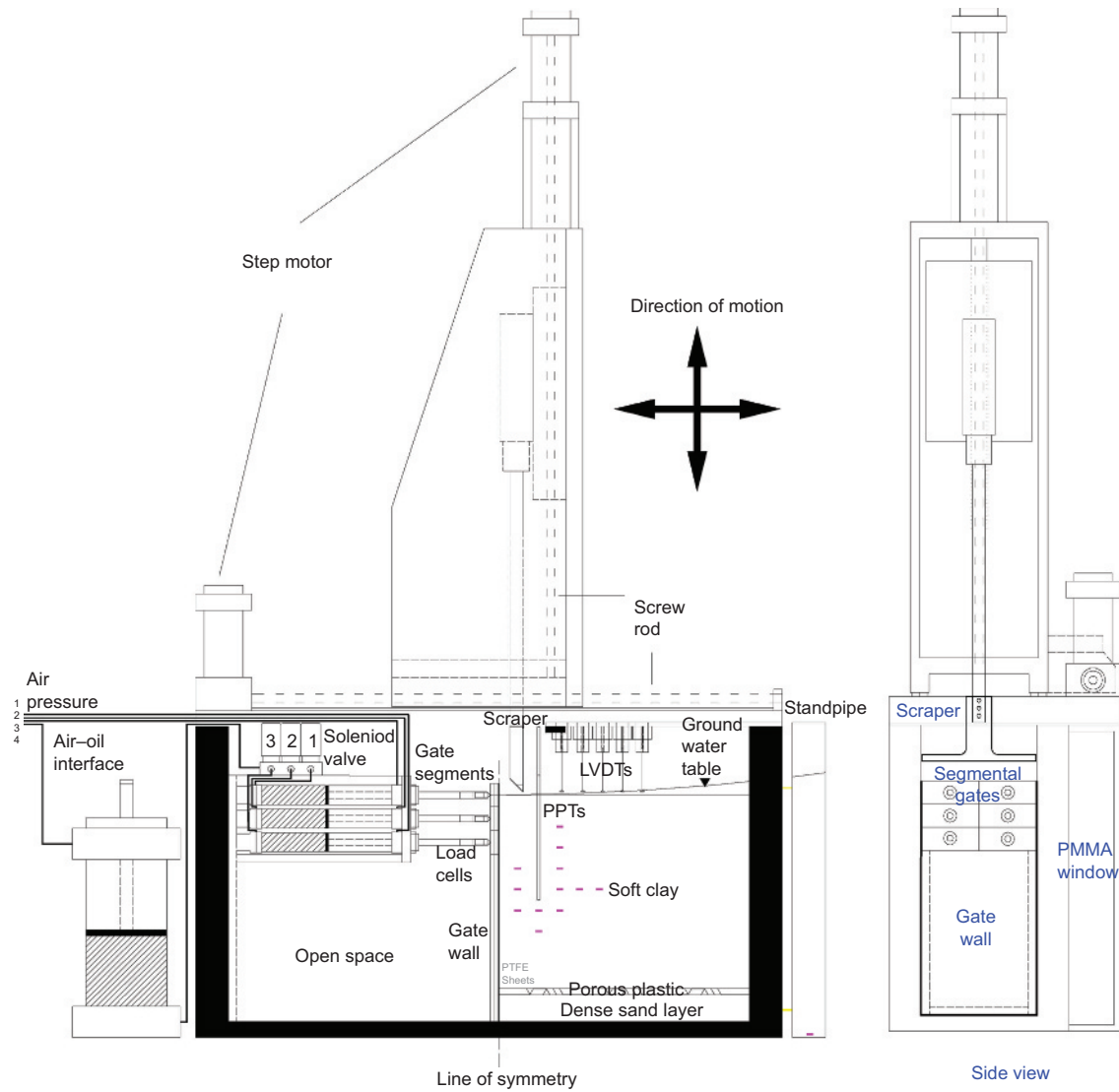


Figure 2. Schematic diagram of experimental set-up with in-flight excavator

achieved by increasing air pressure at the air–oil interface and activating the solenoid valve for that specific pair of props. The propping force can be controlled by adjusting the air pressure at the air–oil interface. That solenoid valve is then closed and the associated props remain stiff owing to the incompressibility of hydraulic oil. On the other hand, retreating cylinders requires the reduction of air pressure at the air–oil interface and the increase in air pressure at the backward pressure inlet of the cylinders.

Figure 4 shows the gate system. At the start of the experiment, three pairs of sacrificial gates, each 36 mm high, sit on the top of the gate wall. They act as a support to retain the soil to be

excavated. The gates are temporarily supported by the pairs of cylinders throughout the initial reconsolidation stage before excavation. The forces required to support the gate segments are monitored by axial load cells attached at the end of each prop. Figure 5 shows the sequence of the first excavation stage. At the start of excavation, the first pair of cylinders is retracted so that the first layer of gates is in an unstable condition and is easily knocked down by the scraper of the in-flight excavator. The in-flight excavator then makes a 4 mm cut into the soil, which is scraped off into the open space inside the cylinder support system. The scraper then returns to its initial position and makes another 4 mm cut, repeating until the excavation level reaches the top of the second level of gates. At that

Centrifuge tests	1	2
	Rigid wall	Flexible wall
Objective	Baseline test	Wall stiffness
Clay depth in model scale: mm	300	300
Prop stiffness: kN/mm	1.66	1.66
Wall stiffness, EI : MNm ² /m	280.4	10.8
System stiffness $EI/\gamma_w s^4$	2860	106

Table 2. A summary of centrifuge testing programme

moment, the first level of props is advanced over the top of the scraper to support the retaining wall. The prop force required can be adjusted by looking at the readings given by the prop load cells. This completes the first stage of excavation. As the scraper is made in an inverted T-shape, it can continue scraping below the first pair of props. The second and third stages of excavation can therefore proceed by repeating the same steps carried out for the first level.

5. Preparation of model ground

Standardisation of experimental procedures is very important as it determines the ability to reproduce similar soil stress states in each experiment. Both clay and sand were used in the present experiments.

A base layer of fine fraction E sand was formed by pluviation using an automatic pouring machine (Madabhushi *et al.*, 2006; Zhao *et al.*, 2006). A constant fall height of 600 mm was used

to achieve a uniform layer with a relative density above 95% and a dry unit weight of 16.0 kN/m³. The properties of the sand are shown in Table 3. The sand was saturated with water by connecting the bottom drainage hole to a standpipe.

Since the objective of these particular tests was to monitor excavation in soft clay and to compare different bracing schemes, lightly over-consolidated kaolin clay was used in the models. A standard procedure was adopted to ensure repetitive reproduction of the model ground with similar strength profiles in each test. Speswhite kaolin clay was chosen for the tests because the parameters are well defined in the literature: some mineralogy and properties are given Table 4. Clay powder was mixed with water to about twice the liquid limit (i.e. 120% moisture content), the mixing taking place under vacuum for at least 2 h. The inner surface of the test container was coated with silicone grease to minimise friction against the clay. The clay slurry was carefully poured on the bearing layer, which consisted of a sheet of filter material placed over the base layer of sand. The final height of the slurry was 550 mm. The container was placed in a hydraulic press, and pressure was applied to the clay in seven loading steps (to 2 kPa, 5 kPa, 10 kPa, 20 kPa, 40 kPa, 80 kPa and 160 kPa).

The final pressure of 160 kPa was intended to achieve an estimated c_u of 25 kPa for the clay at mid-depth in the centrifuge model when it had swollen back into equilibrium at 60g.

When the settlement of the clay in the press became steady under 80 kPa vertical stress, the clay was unloaded. Nine pore

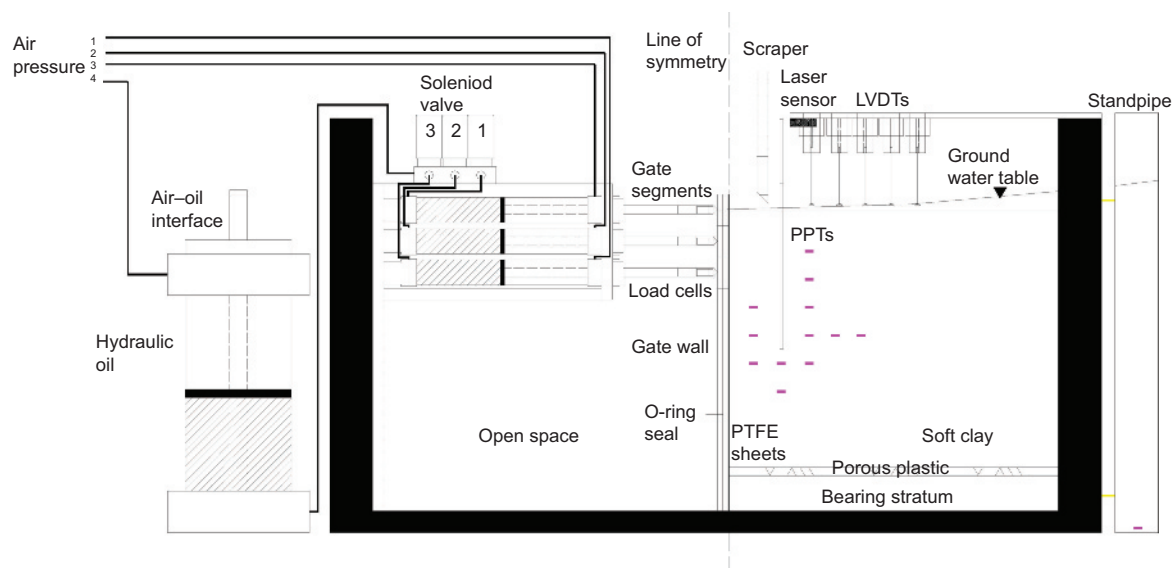


Figure 3. General arrangement of main apparatus

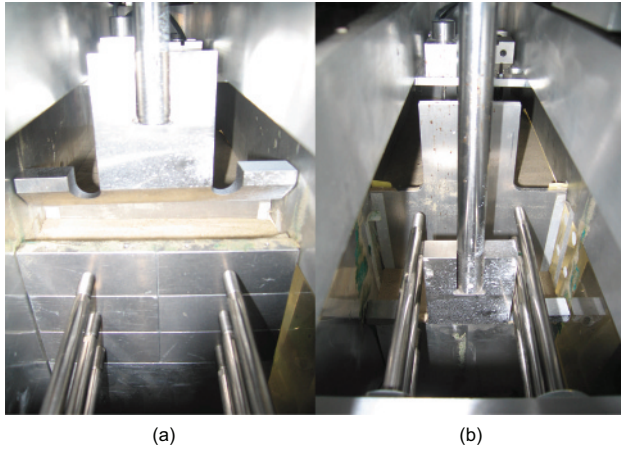


Figure 4. Propping and gate system: (a) before and (b) after excavation

pressure transducers (PPTs) were inserted through pre-drilled openings in the back wall of the container. PPTs were installed through 90 mm long holes augured horizontally into the clay using a hand drill. Unconsolidated slurry was then injected to fill the holes, and the openings were sealed. The final locations of the PPTs are shown in Figure 6(a). The spacing between PPTs was about 30 mm. After installation, the vertical stress was brought back to 80 kPa. After equilibration, the vertical stress was further increased to 160 kPa. After settlement was steady, the stress was reduced again to 80 kPa and the clay was allowed to swell into equilibrium. Removal of this final pressure was known by experience to be possible without drawing air into the clay.

6. Model making and instrumentation

The loading plate was removed. After trimming the clay surface, the resulting clay thickness was 295 mm. The front wall of the model container was then removed. The clay and base layer were then removed from that half of the package

that would contain the cylinder support system. An O-ring seal was placed along the edges of the gate wall to seal the gap at the side walls of the box. The retaining wall, in the particular test to be described here, is made of either a 6 mm or 2 mm thick aluminium alloy plate with an equivalent stiffness (EI) of 280.8 or 10.4 MNm/m² at prototype scale. This wall simulates a 0.5 m thick concrete diaphragm wall or a sheet pile wall (US steel, PDA-27) in the field.

Aluminium alloy was chosen as it is stiff and light. This reduces the effect of excessive settlement of the wall in soft ground during self-weight consolidation. Six slots are made to accommodate total pressure cells (Entran EPL-D1-X-7BAR). The wall was instrumented with bending moment strain gauges arranged in Wheatstone bridges at 32 mm intervals. Greased wiper seals were used to prevent water from seeping past the sides of the wall and to ensure a free sliding condition with minimal friction. The wall was installed at a depth of 160 mm (equivalent to 10.6 m prototype). A set of vertical guides and a cutter were used to dig a trench with the same thickness as the wall. The wall was then pushed into the trench using a vertical guide.

With the clay cross-section uppermost, grains of black-dyed fraction E sand were blown onto the clay to provide texture for image tracking. Lubricant was then applied to the PMMA window to reduce friction against the soil cross-section. The hollow frame, PMMA window and window frame were then bolted to the main body of the container.

Linear variable differential transformers (LVDTs) were assembled at 30 mm spacing intervals from the wall to measure the soil settlement profile of the ground surface. A laser sensor was used to monitor the lateral displacement of the top of the wall. Finally, the water table in the clay was to be maintained at the ground surface by permitting overflow from a standpipe that would be supplied continuously throughout the experiment. Two 8 megapixel cameras took pictures throughout the

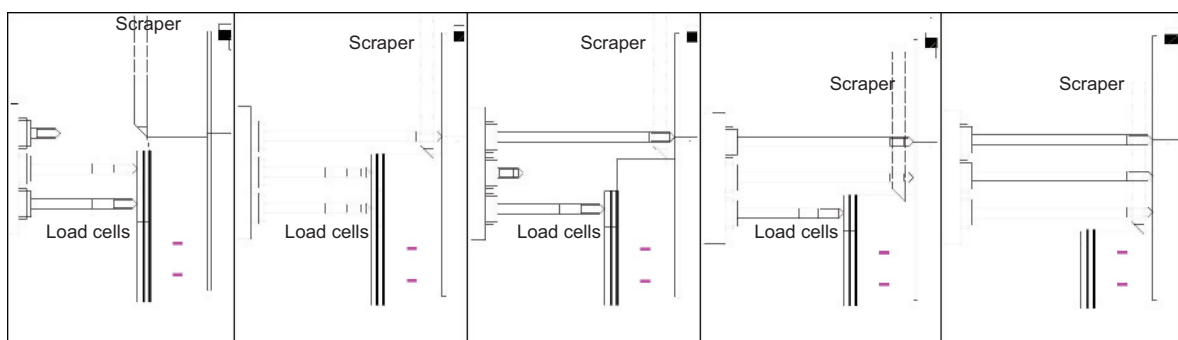


Figure 5. Modelling sequences of excavation

Properties	Value
Minimum void ratio	0.613
Maximum void ratio	1.014
Minimum dry unit weight	12.9 kN/m ³
Maximum dry unit weight	16.1 kN/m ³
Specific gravity of solids	2.65
D_{10}	124 μm
D_{50}	218 μm
D_{60}	360 μm

Table 3. Properties of fraction E sand

Mineralogy/properties	Value
Silicon dioxide (SiO ₂)	47%
Aluminium oxide (Al ₂ O ₃)	38%
300 mesh residue	0.02% maximum
≥10 mm	0.5% maximum
≤2 μm	80 ± 3%
Specific gravity	2.6
Surface area	14 m ² /g
pH	5.0 ± 0.5
Oil absorption	42 g/100 g
Water-soluble salts content	0.2%

Table 4. Mineralogy and properties of Speswhite kaolin

experiment with the provision of suitable lighting. A close-circuit television (CCTV) camera and a webcam were used to observe the behaviour of the propping system during the excavation. The detailed locations of the instruments are shown in Figures 6 and 7.

7. Excavation testing procedures

The in-flight excavator was bolted above the model container, and the integrated assembly was transferred onto the centrifuge swing platform. This was fixed to the torsion-bar catches which permit the package to rotate into a fixed-end condition at a centrifuge acceleration of about 10g. The model was then brought to its scale acceleration of 60g. There are three test phases for a typical centrifuge test of deep excavation–reconsolidation, in-flight excavation and long-term equilibration.

As an increase in soil self-weight leads to an increase in excess pore pressure, the model ground first had to undergo about 5 h of reconsolidation until at least 90% of the consequential consolidation was achieved. The degree of consolidation was monitored by judging whether PPT readings were approaching their hydrostatic state.

The excavation was then started. The in-flight excavator operated at a rate of 5 mm/s horizontally and with 4 mm vertical increments. In order to ensure that realistic quasi-undrained responses were observed, the excavation process should be finished within a reasonably short period of time. Figure 8 shows the progress of excavation in all tests. Excavation to an excavation depth of 5.5 m finished within 72–96 days in prototype scale (30–40 min in model scale), which is similar to the rate of excavation in the field. It is debatable, of course, whether a field profile in typical soft clay with sand and silt layers would be more or less permeable than the kaolin in the model.

Following excavation, the test was allowed to continue and excess pore pressures that had been generated by excavation

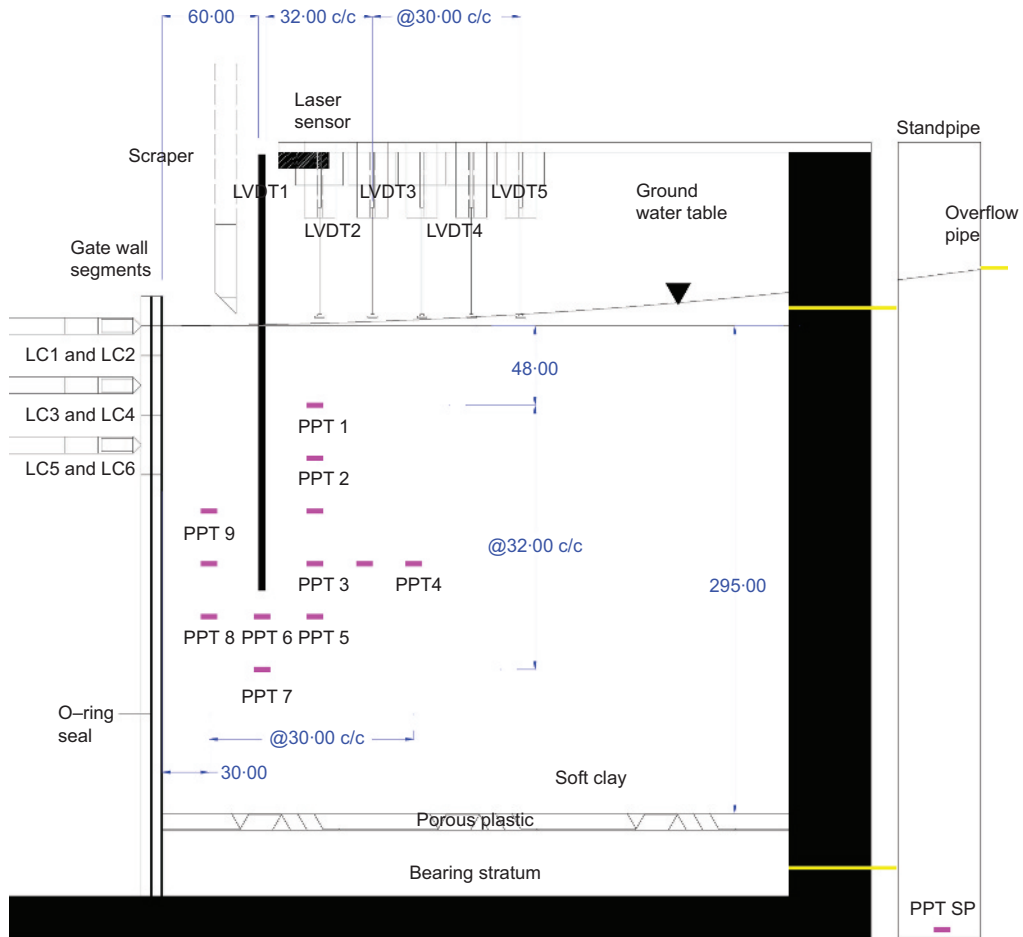
were observed to dissipate as long-term deformations were monitored.

8. Results and discussion

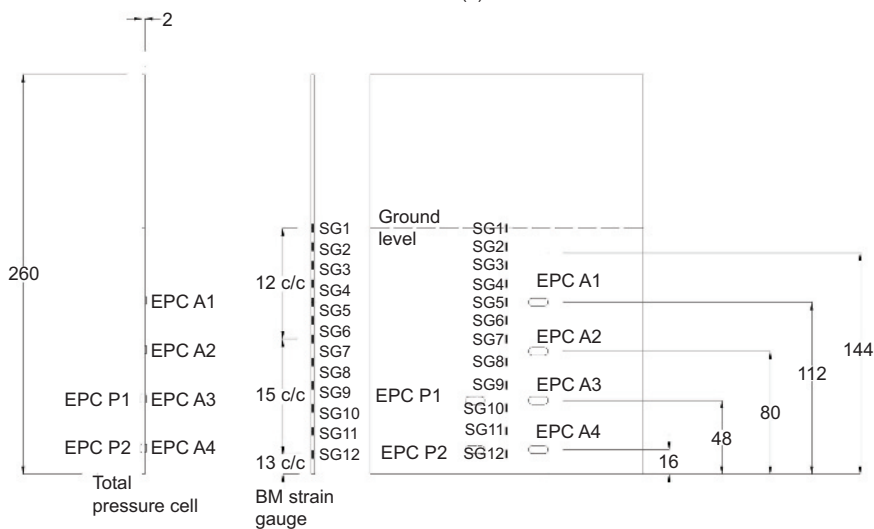
There are three test phases for a typical centrifuge test of excavation. First, the soil sample is allowed to reconsolidate under its enhanced self-weight. Then, in-flight excavation is carried out. Finally, the soil sample is allowed to reconsolidate for dissipation of excess pore pressures generated during the excavation stage.

Figure 9 shows the response in pore water pressure, bending moment and ground settlement with respect to time for a typical excavation test. During the spin-up, excess pore water pressures were generated owing to the enhanced self-weight of the soil. The soil sample was then allowed to consolidate and pore water pressure approached hydrostatic equilibrium after 5 h (Figure 9(a)). Similarly, the surface settlement stabilises after the dissipation of excess pore water pressure is complete (Figure 9(b)). During the reconsolidation phase, bending moments observed in the retaining wall were found to remain minimal, as required (Figure 9(c)). Richards and Powrie (1998) reported that some bending moments were observed during their reconsolidation phase, amounting to more than 20% of the later excavation-induced bending moments. This was attributed to the mismatch between the total horizontal stress profile in the soil and the hydrostatic pressure in the heavy fluid used to support the wall. Thus, the wall retaining heavy fluid bends to fulfil the force equilibrium requirement. No such problem has occurred with the new actuation system.

With the benefit of a time-scaling factor of n^2 for consolidation problems in the centrifuge, the long-term behaviour of the retaining wall system is investigated. Dissipation of excess pore water pressure is allowed owing to water discharge from the double drainage boundaries, which eventually leads to a constant seepage condition around the wall toe. Swelling and



(a)



(b)

Figure 6. Positions of instruments: (a) elevation view; (b) plan view (dimensions in model scale in mm)

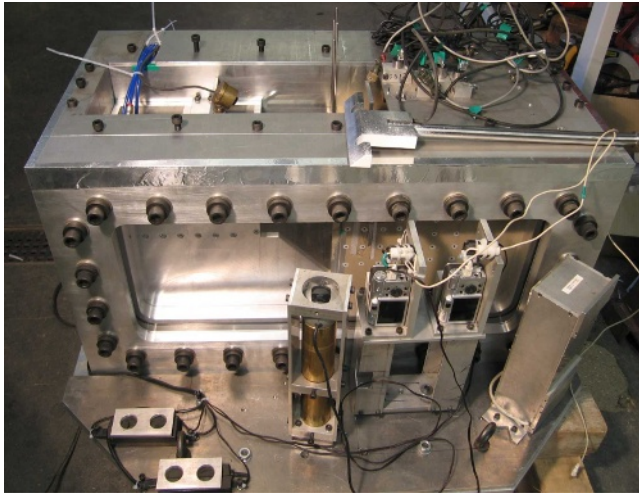


Figure 7. Configuration of PIV cameras and webcam (front)

softening of the soft clay occurs on the excavation side owing to the removal of the overburden stress and the up-welling of ground water. This leads to the redistribution of total horizontal stress along the wall.

8.1 Apparent earth pressure

The design of bracing systems usually involves the calculation of prop forces using apparent earth pressure envelopes developed empirically by Peck (1969) from field measurement of maximum strut forces and tributary areas of soil, which were obtained from early projects supported by sheet pile or soldier pile and lagging walls in the 1960s. Figure 10(a) shows the development of measured average earth pressure profiles calculated from the ratio of the measured prop load to the tributary area for each prop (i.e. horizontal prop spacing \times vertical prop spacing). The maximum strut force is usually observed just before the installation of the next deeper level of strut. Strut forces at higher elevations would then usually relieve.

Hashash and Whittle (2002) propose that an arching mechanism forms with the major principal stresses directed toward the lowest level of strut, while an underlying compressive arch also transfers load onto the embedded section of the wall. After installation of the lowest strut, a deeper arching mechanism forms. This agrees well with the centrifuge observation that the apparent earth pressure drops after installation of the lowest prop. Figure 10(b) shows the profile of apparent earth pressure at an excavation depth of 5.5 m, with three levels of bracing above. The measured pressures are compared with Peck's design recommendations for soft to firm clay. The model data clearly show the influence of structural stiffness. The maximum apparent earth pressure for depths beyond 25% of the final excavation depth can, according to Peck (1969), be taken as

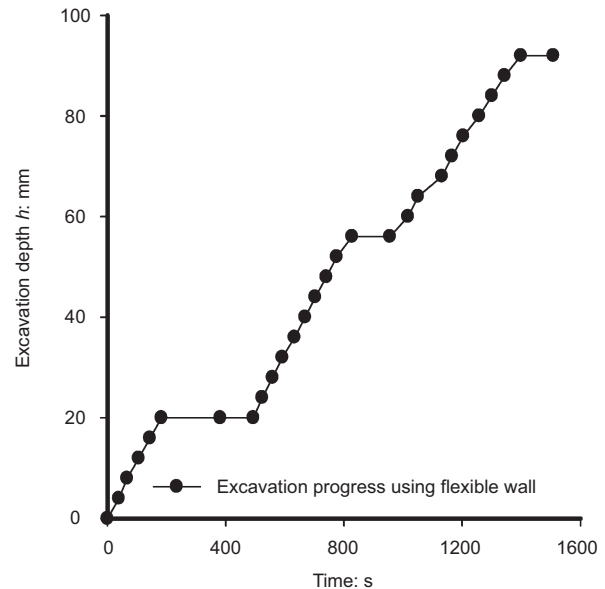


Figure 8. Progress of excavation

$$1. \quad \sigma_h^A = K_a \gamma_t H \quad \text{with} \quad K_a = 1 - m \left(\frac{4s_u}{\gamma_t H} \right)$$

where γ_t is the representative unit weight of the soil, s_u is the undrained shear strength averaged over the depth of excavation and the factor m is 0.4.

Results show that the recommended design values agree with the measurements in the top 2 m of soils for all cases. However, the recommended values under-predict the values measured below the top struts by 30% for the case of excavations supported by diaphragm walls. Similar findings were reported for excavations supported by stiff well-embedded diaphragm walls in numerical studies by Goldberg *et al.* (1976) and Hashash and Whittle (2002). On the other hand, reducing the bending stiffness of the retaining wall or axial stiffness of the propping system causes a reduction in apparent earth pressures and a close agreement with Peck's design envelope as revealed in Figure 10(b).

8.2 Pore pressure behaviour

As the excavation proceeded, the ground water level in front of the wall was lowered simultaneously with the soil. However, the bottom drainage layer was connected throughout each test to a standpipe which maintained a hydrostatic water pressure measured from the soil surface at the back of the wall. Water flow past the sides of the wall was prevented by greased seals. Under such conditions, downward seepage should ultimately be expected at the back of the wall providing upward seepage

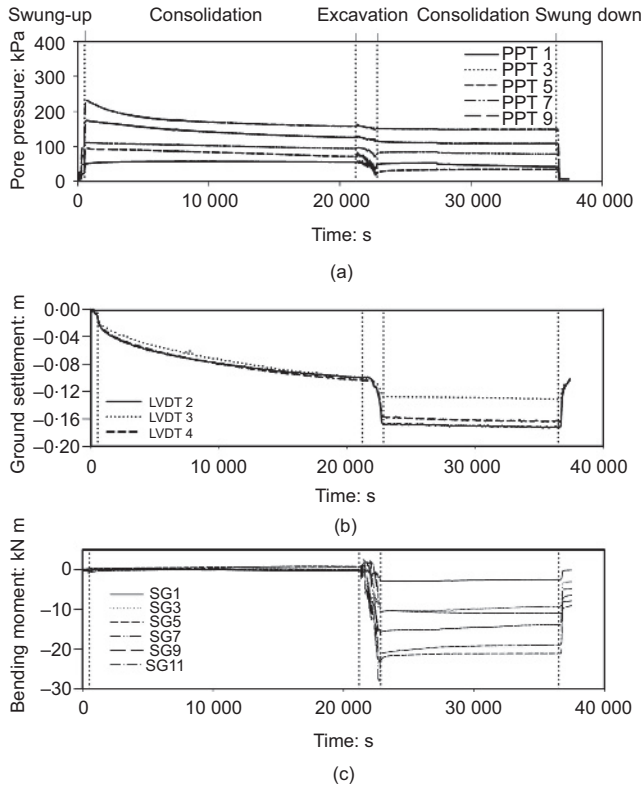


Figure 9. Typical centrifuge test responses for: (a) pore water pressure; (b) ground settlement; (c) bending moment on retaining wall

in front of the wall. However, transient pore pressures must be expected during the excavation process.

Figure 11 shows the variation of pore water pressure observed for different instances of time as the excavation progressed, using a sheet pile wall in test 2. The variation of pore pressure with depth at different stages of excavation is shown in Figure 11. In front of the wall, a negative pore pressure built up (PPT 9 and PPT 8) due to the reduction in total mean stress induced by the excavation. The reduction in total vertical stress in the passive zone is also plotted in the same figure for comparison. However, the magnitude of the negative pore pressures was less than half of the effective overburden pressure lost by excavation. This is attributed to the negative pore pressure being partially cancelled by positive pore pressures generated by shear deformation of soft clay. On the other hand, the changes in pore pressure measured at the back of the retaining wall (PPT 1, PPT 2, PPT 3, PPT5 and PPT6) were relatively small because the stiff prop supports limited lateral wall deformation, and thus limited any reduction in lateral horizontal stress.

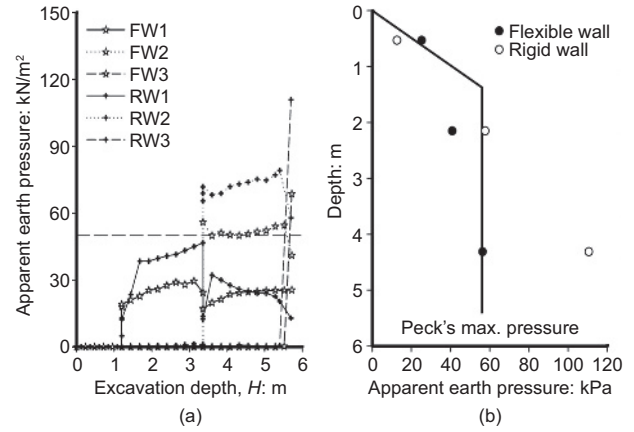


Figure 10. Development of prop forces during excavation: (a) with excavation depth; (b) with depth

In the long term, the dissipation of excess pore water pressure leads to the long-term steady-state seepage condition. The drainage path at the particular location of the PPTs governs the rate of excess pore pressure dissipation accordingly. In general, all the readings stabilise for the development of steady seepage condition after 200 days. For the present studies, since the pore pressure within the bottom drainage layer is maintained as hydrostatic with a water table at the ground surface, this would represent cases of excavation site where there is a high-pressure water aquifer located below the soft clay stratum. Design against hydraulic failure would become a critical issue for engineers. The pore water pressure on the retained side recovers to slightly lower than its original level owing to seepage effects. Most importantly, the pore water pressure inside the excavation drops tremendously due to the drawdown of water table in the pit, as would be achieved by dewatering. Both soil softening in the excavation pit owing to overburden vertical stress removal with consolidation and seepage forces lead to a reduction in passive resistance of the soil in the excavation pit. This would possibly cause gradual long-term wall toe kick-out scenarios.

8.3 Earth pressures

The variation of measured total earth pressure during excavation and the final earth pressure profile on both sides of the sheet pile wall are shown in Figures 12 and 13 respectively. In Figure 13, the pressure under K_0 conditions before excavation and Rankine's active and passive pressure at an excavation depth of 5.5 m are also presented. In the calculation of Rankine's pressure, an undrained condition is assumed with an estimated undrained shear strength of 27 kPa using the empirical correlation by Jamiolkowski *et al.* (1985) defined as follows

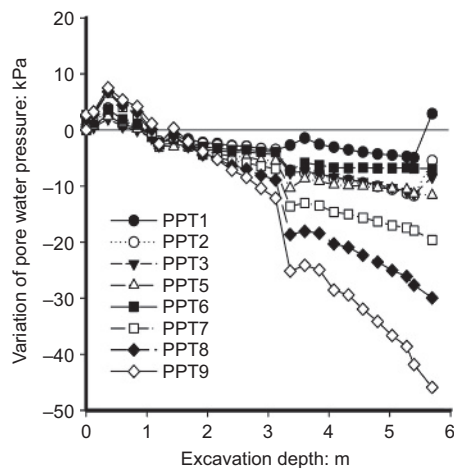


Figure 11. Variation of pore water pressure with excavation depth

$$2. \quad c_u = 0.22\sigma_v'(\text{OCR})^{0.8}$$

At the back of the wall, there is a gradual decrease in total pressure with excavation depth. As the excavation depth increases, a larger decrease in total pressure is observed owing to deep-seated soil movement below the lowest prop. At the front of the wall, there are two opposing effects, a decrease in total earth pressure owing to the removal of soil and an increase due to the progressive mobilisation of passive pressure.

Effective earth pressure coefficient is derived from the earth pressure cell data and the pore pressure data with the assumption of constant vertical total stress on a stress element at a depth throughout the excavation process. K is calculated as follows

$$3. \quad K = \frac{\sigma_h - u}{\gamma_{\text{sat}}d - u}$$

where σ_h , γ_{sat} , d and u are total horizontal stress measured by earth pressure cell, saturated unit weight, depth of pressure cell and pore water pressure measured by pore pressure transducer, respectively.

As shown in Figure 14(a), in the early stage of excavation the earth pressure in front of the wall registered by stress cell EPC P1 (Figure 6(b)) stays constant ($h < 0.5 H_f$ where h and H_f are the excavation depth and the final excavation depth, respectively) but it eventually drops with an increasing rate as the excavation progresses to full depth ($h > 0.5 H_f$). For the simulation method of excavation using heavy fluid, K within

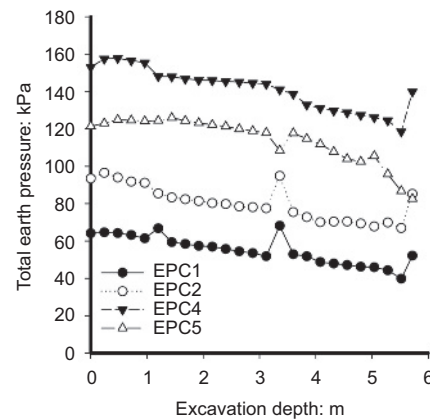


Figure 12. Variation of total pressure with depth of excavation

the zone of future excavation will in theory remain at unity, which is not consistent with what happens in the field where K below the excavation level may approach the passive earth pressure coefficient K_p as shown in Figure 14(b). Thus, the technique of using heavy fluid does not accurately reproduce the prototype deformations and stresses with respect to the progress of excavation. This confirms the necessity of excavating real soil in-flight, rather than draining heavy fluid, if pressures and bending moments are to be precisely simulated.

8.4 Observed bending moment

Figure 15 shows the development of bending moment per metre run during in-flight excavation in a deep clay stratum. For the first stage of unpropped excavation, negative bending moments developed near the toe of the cantilever wall. After introduction of the first layer of struts, the wall was allowed to rotate about the wall crest and developed a bulge below the excavation. Positive bending moments therefore developed. On the other hand, installation of deeper props induced a slight reduction of wall bending moments at higher elevations. As the excavation proceeded, the lateral restraint imposed by the support system on the retaining wall led to the development of a deep-seated deformation mechanism below the lowest strut. Positive bending moments were induced below the lowest props. The maximum bending moment induced by the undrained excavation amounted to about 200 kNm/m. In the long term, after swelling, the magnitude of maximum bending moment decreased to 150 kNm/m as a result of the clay softening and stress redistribution on the excavation side. In the long term it is the overall stability of the softening clay, rather than the bending moments and reactions in the supporting structure, that are the cause for concern in excavations that have been left open to groundwater flow.

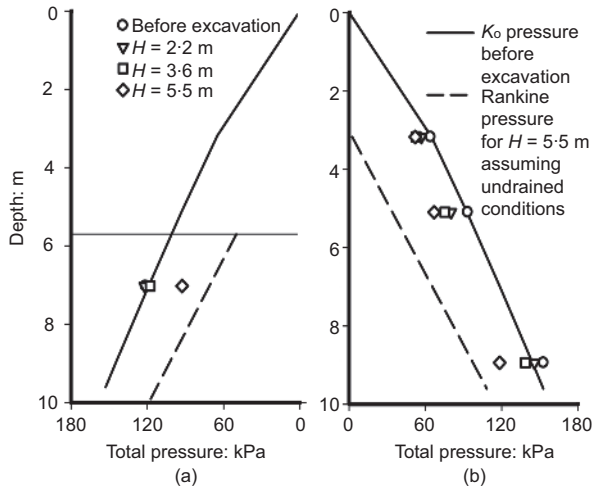


Figure 13. Distribution of total pressure on: (a) excavation side; (b) retained side

8.5 Ground settlement and wall displacement

The magnitude of wall deflection and the ground settlement profile during undrained excavation are vital in assessing potential damage to neighbouring structures and buried services. In an ideal excavation process, the first level of support is installed at an early stage in order to minimise cantilever deflections. However, this may not always be possible in practice owing to a variety of site constraints and construction sequences. In the present studies, the excavation procedures initiated with a cantilever stage of excavation, which was then followed by singly propped and finally multi-propped excavation stages. Ground movements were captured by the particle image velocimetry (PIV) technique. Some discrete measurements monitored by LVDTs are included for comparison. In general, the results obtained by LVDTs and the PIV technique are comparable, which confirms that the model is deforming under plane strain conditions.

Figure 16 shows the PIV results of lateral wall displacement and ground settlement developing around a deep excavation supported by a flexible sheet pile wall. The PIV results are compared with the LVDT data to ensure a plane strain testing condition in Figure 16. Consistent with results shown by previous researchers (Powrie, 1986), a rotation of the wall about its toe was observed in the cantilever excavation stage. A maximum incremental prototype cantilever wall deflection of about 10 mm was inferred at the wall crest (0.167 mm at model scale), which is equivalent to 0.2% of average engineering shear strain in the 45° triangular zone behind the wall (as shown in Figure 17(a)) according to Osman and Bolton (2004). The settlement trough extends some way

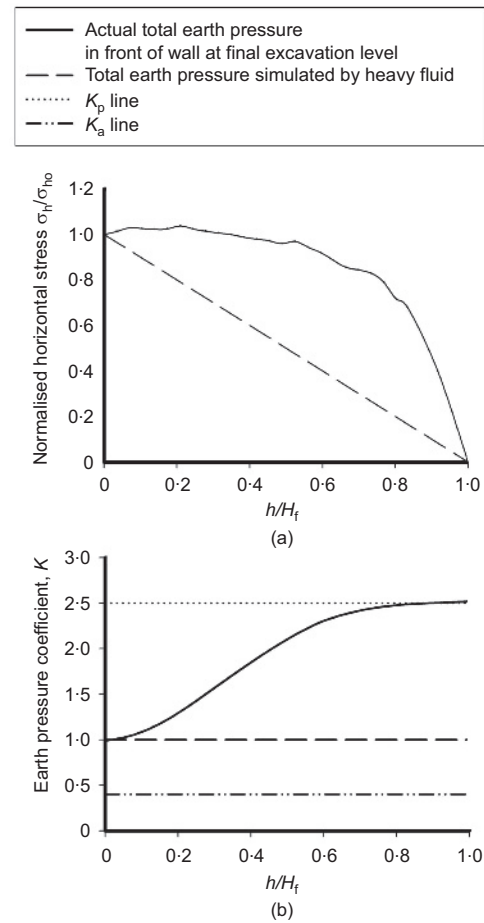


Figure 14. Variation of (a) normalised horizontal earth pressure and (b) earth pressure coefficient with normalised excavation depth

beyond the triangular trough pattern observed by Powrie (1986). The subsequent stages of excavation involve a deep-seated soil flow mechanism (shown in Figures 17(b) and 17(c))

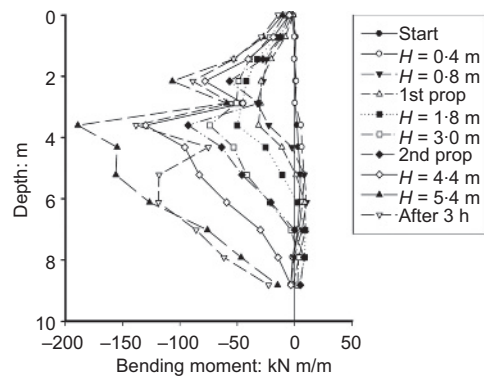


Figure 15. Development of bending moment

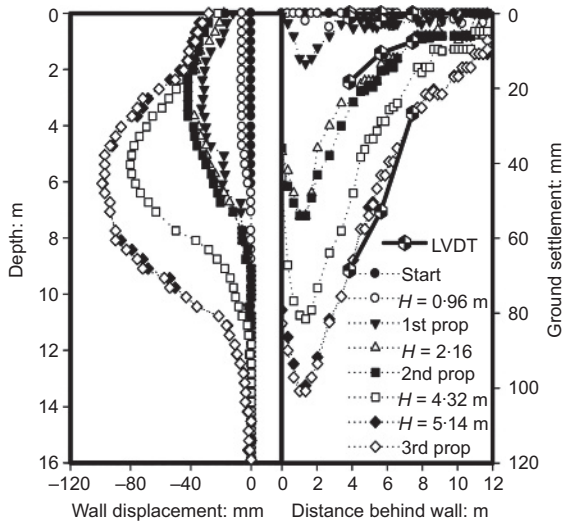


Figure 16. Development of lateral wall displacement and ground surface settlement during excavation

and bulging of the retaining wall below the lowest level of struts. The maximum incremental lateral wall displacements for the second and the third stages were 30 mm and 90 mm (0.5 mm and 1.5 mm at model scale), respectively. These movements were, respectively, equivalent to about 0.6% and 1.5% of average incremental engineering shear strain within the deformation zone, according to Bolton *et al.* (2008). These findings emphasise the importance of soil stiffness measured prior to failure, when attempting to predict the deformations around multi-propped excavations.

The development of the settlement profile in Figure 16 is characterised by the development of a deep settlement trough near the wall. It is also consistent with the observation of Clough and O'Rourke (1990) that the settlement trough of a multi-propped excavation is bounded by a trapezoidal zone extending up to two times the maximum excavation depth. It is also noted that the area swept by the retaining wall is roughly equal to the area underneath the settlement trough, consistent with zero volumetric strain in the undrained conditions of rapid excavation in clay.

9. Conclusions

Centrifuge model tests of excavations in lightly over-consolidated clay were carried out using a newly developed actuation system which could simulate a realistic sequence of excavation and propping. The new method provides appropriate initial ground conditions before excavation starts, so that no pre-excavation bending moments develop during reconsolidation. The actual removal of soil also enables the realistic, progressive development of passive resistance on the excavation side. The previously favoured centrifuge modelling technique of draining heavy fluid as a substitute for soil removal suffers from the introduction of pre-excavation lateral wall movements and bending moments, and also imposes a constant earth pressure coefficient of unity in the zone of excavation, which distorts the responses of model retaining systems. Nevertheless, the simple techniques such as draining of heavy fluid would offer a quick and easy alternative modelling technique though compromising a certain degree of accuracy, whereas an in-flight excavator required demanding efforts and resources in the development of equipment.

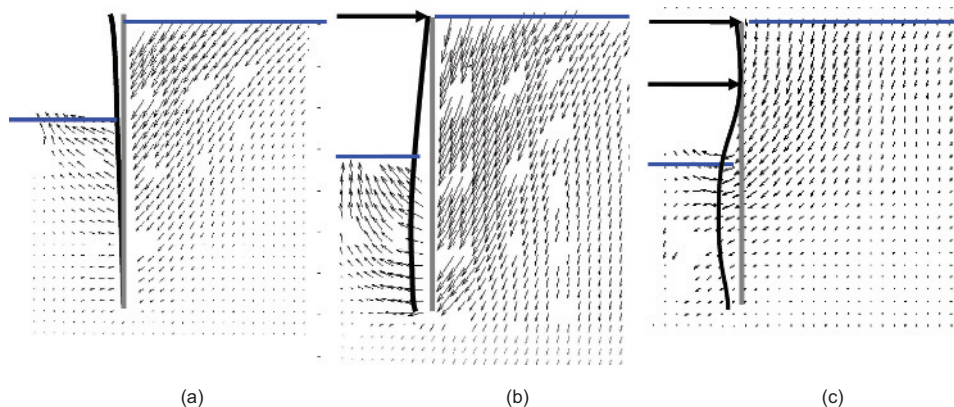


Figure 17. Incremental deformation mechanism observed for different stages of excavation (length of vectors not to scale): (a) cantilever stage; (b) prop installed at crest; (c) multi-propped stage

The performance of a typical model excavation procedure was monitored using a variety of instruments. Changes in prop loads, pore pressures, total earth pressures, ground settlements and bending moments on the retaining wall were successfully demonstrated. Results confirm that stiffer retaining systems attract higher apparent earth pressure than a flexible retaining system. Negative excessive pore water pressures induced by excavation were smaller than might have been expected from purely elastic unloading. This was attributed to positive pore pressure increments generated from shearing the soft soil; these ultimately alter the drained swelling response. In addition, the development of bending stresses in the retaining wall was obtained in both the short and long term. Finally, and most usefully, digital image analysis using the PIV technique enabled the development of the complete soil deformation mechanism to be displayed as an incremental process dependent on the propping conditions applicable during each stage of excavation. The accuracy of PIV in determining the development of lateral wall movements and ground settlements was cross-checked by the use of LVDTs, and plane strain test conditions were confirmed. The observed deformation mechanisms confirm that a potentially damaging settlement trough could develop in the retained soil well before the mobilisation of peak soil strength, and well before failure of the retaining wall. The practical importance of knowing the soil stiffness prior to failure is therefore emphasised. Quick and efficient methods of predicting ground movements, based on such observed deformation mechanisms, are becoming available (Bolton *et al.*, 2008; Lam and Bolton, 2011).

Acknowledgements

The authors would like to thank all staff at the Schofield Centre, and especially the technicians, Steve Chandler, John Chandler, Richard Adams, Kristian Pether and Chris McGinnie for their help with the experimental set-up. The authors would also like to acknowledge the Platform grant (GR/T18660/01) awarded by the UK Engineering and Physical Sciences Research Council.

REFERENCES

- Azevedo RF (1983) *Centrifuge and Analytical Modelling of Excavation in Sand*. PhD thesis, University of Colorado, Boulder, CO, USA.
- Bolton MD and Powrie W (1987) The collapse of diaphragm walls retaining clay. *Géotechnique* **37**(3): 335–353.
- Bolton MD, Lam SY and Osman AS (2008) Supporting excavations in clay – from analysis to decision-making. Special Lecture. *Proceedings of the 6th International Symposium of Geotechnical Aspects of Underground Construction in Soft Ground*, Shanghai, pp. 15–28.
- Clough GW and O'Rourke TD (1990) Construction induced movements of in situ walls. In *Design and Performance of Earth Retaining Structures* (Lambe P and Hansesn LA (eds)). ASCE, New York, NY, USA, Geotechnical Special Publication no. 25, pp. 439–470.
- Goldberg DT, Jaworski WE and Gordon MD (1976) *Lateral Support Systems and Underpinning*. Federal Highway Administration, Washington, DC, USA, Report FHWA-RD-75-128.
- Haigh SK, Houghton NE, Lam SY, Li Z and Wallbridge PW (2010) Development of a double-axis servo-actuator for novel centrifuge modeling. *Proceedings of ICPMG 2010*, Zurich, Switzerland, pp. 239–244.
- Hashash YMA and Whittle AJ (2002) Mechanisms of load transfer and arching for braced excavations in clay. *Journal of Geotechnical and Geoenvironmental Engineering, ASCE* **128**(3): 187–197.
- Jamiolkowski M, Ladd CC, Germaine JT and Lancellotta R (1985) New developments in field and laboratory testing of soils. *Proceedings of the 11th ICSMFE*, San Francisco, CA, USA, vol. 1, pp. 57–153.
- Kimura T, Takemura J, Hiro-pka A, Suemasa N and Kouda N (1993) Stability of unsupported and supported vertical cuts in soft clay. *Proceedings of the 11th SEAGC*, Singapore, pp. 61–70.
- Lam SY and Bolton MD (2011) Energy conservation as a principle underlying mobilizable strength design for deep excavations. *Journal of Geotechnical and Geoenvironmental Engineering, ASCE* **137**(11): 1062–1074.
- Loh CK, Tan TS and Lee FH (1998) Three dimensional excavation tests in the centrifuge. *Proceedings of Centrifuge 98*, Tokyo, Japan, pp. 649–652.
- Lyndon A and Schofield AN (1970) Centrifuge model test of short term failure in London clay. *Géotechnique* **20**(4): 440–442.
- Madabhushi SPG, Houghton NE and Haigh SK (2006) A new automatic sand pourer for model preparation at University of Cambridge. *Proceedings of ICPMG 2006*, Hong Kong, pp. 217–222.
- Osman AS and Bolton MD (2004) A new design method for retaining walls in clay. *Canadian Geotechnical Journal* **41**(3): 453–469.
- Peck RB (1969) Deep excavation and tunnelling in soft ground. *Proceedings of the 7th ICSMFE, State-of-the-art Volume*, Mexico City, Mexico, pp. 225–290.
- Powrie W (1986) *The Behavior of Diaphragm Walls in Clay*. PhD thesis, University of Cambridge, UK.
- Richards DJ and Powrie W (1998) Centrifuge model tests on doubly propped embedded retaining walls in over-consolidated kaolin clay. *Géotechnique* **48**(6): 833–846.

Richards DJ, Clark J and Powrie W (2006) Installation effects of a bored pile wall in overconsolidated clay. *Géotechnique* **56(6)**: 411–425.

Takemura J, Kondoh M, Esaki T, Kouda and M Kusakabe (1999) Centrifuge model tests on double propped wall

excavation in soft clay. *Soils and Foundations* **39(3)**: 75–87.

Zhao Y, Gafar K, Elshafie MZEB *et al.* (2006) Calibration and use of a new automatic sand pourer. *Proceedings of ICPMG 2006*, Hong Kong, pp. 265–270.

WHAT DO YOU THINK?

To discuss this paper, please email up to 500 words to the editor at journals@ice.org.uk. Your contribution will be forwarded to the author(s) for a reply and, if considered appropriate by the editorial panel, will be published as discussion in a future issue of the journal.

International Journal of Physical Modelling in Geotechnics relies entirely on contributions sent in by civil engineering professionals, academics and students. Papers should be 2000–5000 words long (briefing papers should be 1000–2000 words long), with adequate illustrations and references. You can submit your paper online via www.icevirtualibrary.com/content/journals, where you will also find detailed author guidelines.